JOURNAL OF MATERIALS SCIENCE 22 (1987) 2975–2982

Electrical properties of zirconium bis(monohydrogen phosphate)monohydrate and its related compounds in a humid atmosphere

Y. SADAOKA, M. MATSUGUCHI, Y. SAKAI, S. MITSUI
Department of Industrial Chemistry, Faculty of Engineering, Ehime University, Matsuyama 790, Japan

Humidity-impedance characteristics were examined for amorphous and crystalline zirconium phosphate. The impedance of crystalline zirconium phosphate is lowered with decreasing particle size. While the impedance of amorphous zirconium phosphate increases steeply with an increase in the burning temperature, the impedance is poorly dependent on burning temperature for crystalline zirconium phosphate in a humid atmosphere. Fine-grained crystalline zirconium phosphate is a suitable material for use as a humidity sensing device because of its humidity sensitivity and response to humidity changes. The existence of amorphous phases is responsible for the increase in response time.

1. Introduction

A wide variety of uses has been found for synthetic organic and inorganic electrolytes. Recently, it has been confirmed that insoluble organic polyelectrolyte is a suitable material for use as a conventional humidity sensing device [1, 2], where thermal stability is not enough. It is expected that insoluble inorganic polyelectrolyte will have a superior thermal stability to organic polyelectrolyte. It is well known that the inorganic electrolytes are formed by polybasic acids and certain hydrolysable polyvalent cations; many of these salts are extremely insoluble in most reagents, typical examples are the phosphates of zirconium and titanium. Of these the zirconium *bis*(monohydrogen orthophosphate)monohydrate, $Zr(HPO_4)_2 \cdot H_2O$, which has a layered structure, is known as an insoluble ion exchange and proton conductor. It has been reported that the specific conductance of zirconium phosphate was enhanced by the adsorption of water [3–5].

It is expected that zirconium phosphate will prove to be a suitable material for use as a humidity sensing device. This paper presents the results of a study of the effects of the structure of zirconium phosphate and of heat treatment on electrical properties in a humid atmosphere.

2. Experimental procedure

Various types of zirconium phosphate were prepared by different methods: (i) precipitation of zirconium phosphate by adding an appropriate amount of phosphoric acid to zirconyl chloride solution (amorphous zirconium phosphate; AZP), (ii) refluxing of amorphous zirconium phosphate with phosphoric acid (CZP100: refluxing time 100 h; CZP400: refluxing time 400 h), (iii) precipitation of zirconium phosphate by adding phosphoric acid to zirconium fluorate solution in a bubbling stream of nitrogen gas (FZP). All the products were washed with distilled and deionized water and dried at 60° C.

The pulverized powder (400 mg) was pressed into discs at 200 kg cm^{-2} which were then shaped to 10 mm × 10 mm. Some discs ~0.5 mm thick were burnt at various temperatures for 3 h in the atmosphere. Next, gold electrodes, 4 mm × 4 mm, were applied to opposite faces of the disc by vacuum evaporation. The crystalline phases were identified at room temperature by the standard X-ray diffraction technique. The microstructure of the discs was examined using scanning electron microscopy and the pore size distribution was determined by means of mercury penetration porosimetry. The specific surface area was determined by the BET method using nitrogen as a sorbate in a stream of helium gas. The concentration of strongly acidic proton was determined by the pH titration method with 0.1 N NaOH solution. The thermal stability and the degree of hydration were examined using a thermal gravimetric analysis in a stream of helium gas.

The humidity dependence of the electrical properties was measured using LCZ meters (100 Hz to 1 MHz). Humidities (% r.h.), ranging from 0 to 90, were prepared by mixing dry and moist air in controlled proportions at 30° C. Stational humidity is achieved within 2 min after setting a certain humidity.

3. Results

3.1. pH titration

The titration curves of CZP and FZP were found to be in fair agreement with the results reported by Clearfield *et al.* [8]. During titration of the suspended solution with 0.1 N NaOH solution, two neutralization points were confirmed at pH 5.0 and pH 8.5 for CZP100 and FZP in which the burning temperature was less than 400° C, no apparent neutralization points could be confirmed for samples burnt at 600° C

0022–2461/87 $03.00 + .12

TABLE I Concentration of strongly and weakly acidic protons and surface area

Sample	Burning temp. (°C)	C_{HS} (mmol g^{-1})	C_{HW} (mmol g^{-1})	Surface area (m^2 g^{-1})
AZP	60	1.70	1.90	23.0
	300	1.10	1.10	68.0
	600	0.30	0.30	56.0
	900	0.05	0.05	1.6
CZP100	60	3.25	3.50	7.3
	300	3.25	3.40	9.2
	600	0.12	0.15	9.5
	900	0.03	0.05	6.0
CZP400	60	3.10	3.42	5.8
	300	3.25	3.55	5.8
	600	0.11	0.06	6.4
	900	0.01	0.05	4.0
FZP	60	3.30	3.30	3.0
	300	3.30	3.25	3.1
	600	0.10	0.10	3.2
	900	0.05	0.05	2.5

or above. For AZP, no distinct neutralization points could be confirmed. From the titration curves, it is considered that at least two types of acidic protons exist on the samples; thus the concentration of strongly acidic proton can be estimated by the point of pH 5.0, and that of the weakly acidic proton by the point of pH 8.5. The concentrations of the strongly acidic proton, C_{HS}, and the weakly acidic proton, C_{HW}, are summarized in Table I. It is clear that the concentrations of both types of acidic proton decrease with increasing burning temperature.

3.2. Thermal gravimetric analysis

To examine the thermal stability and the degree of hydration, thermogravimetric analysis was applied to the samples dried at 60° C at a heating rate of 8° C min^{-1} in a stream of helium gas (40 ml min^{-1}) up to 800° C. For CZP and FZP, two plateau regions were confirmed. On the other hand, for ZAP, no distinct plateau regions could be detected in the temperature

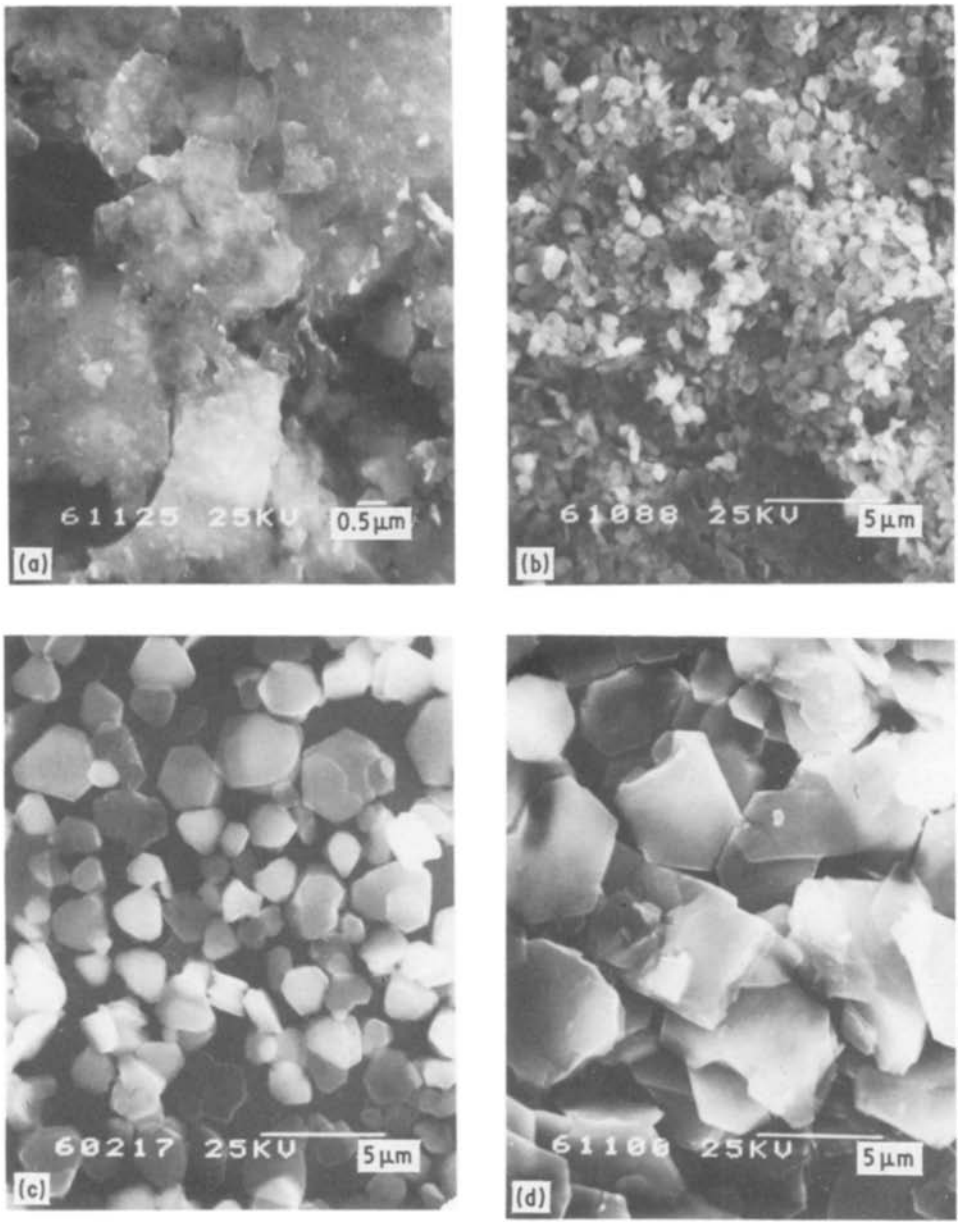

Figure 1 Scanning electron micrographs of discs dried at 60° C. (a) AZP, (b) CZP100, (c) CZP400, (d) FZP.

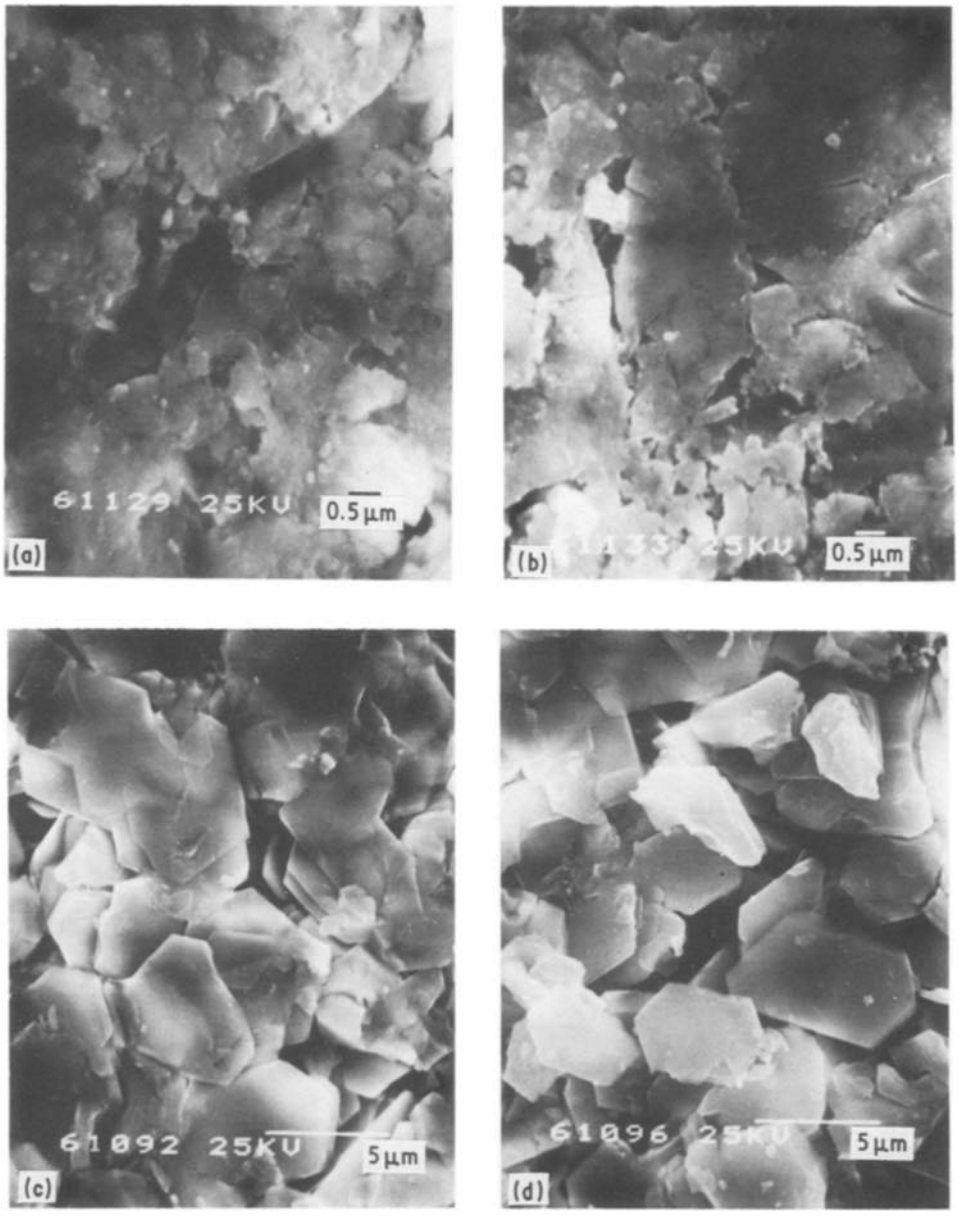

Figure 2 Scanning electron micrographs of discs: (a) AZP burnt at 600° C, (b) AZP burnt at 1000° C, (c) FZP burnt at 600° C, (d) FZP burnt at 1000° C.

region between 60 and 500° C. In addition, no distinct weight loss was confirmed in the region above 600° C for CZP and FZP and above 650° C for AZP.

3.3. Form of the sample

The microstructures of samples dried at 60° C are shown in Fig. 1. For AZP, no apparent crystallized particles could be seen. This observation convinced us that the results of X-ray diffraction analysis were correct, i.e. no peaks were detected. On the other hand, for CZP and FZP, it is clear that the sample requires a good layered crystalline structure. The average particle diameter of the samples dried at 60° C is estimated to be 0.55 μm (CZP100). 2.41 μm (CZP400) and 5.8 μm (FZP), respectively.

For the compressed powder discs burnt at various temperatures, the microstructures are shown in Fig. 2. While for AZP, the new crystalline phases appeared on burning, and the surface area steeply decreased with an increase in burning temperature, no distinct variations of particle form and size being seen in CZP and FZP. These tendencies were confirmed by pore-size distribution measurements (Fig. 3), and surface-area measurements (Table I).

3.4. Complex impedance analysis

A typical complex impedance plot is shown in Fig. 4. In general, the high-frequency results are represented by depressed semicircles, all of which pass through the origin. In addition, at low-frequencies, a second arc or spur was observed in the high humidity region. This spur may arise from the interfacial polarization. The observed results may be represented by an appropriate equivalent circuit as shown in Fig. 4, in which the component corresponding to interfacial polarization is omitted for simplicity. A depressed semicircle appearing in the high frequency region in the complex impedance plot can be adequately expressed by Equation 1:

$$Z(\omega) = Z_0/1 + (j\omega/\omega_0)^{(1-\alpha)} \quad (1)$$

where $Z(\omega)$ is the complex impedance at an angular frequency ω, Z_0 the low frequency, real-axis intercept, ω_0 the relaxation angular frequency at the maximum

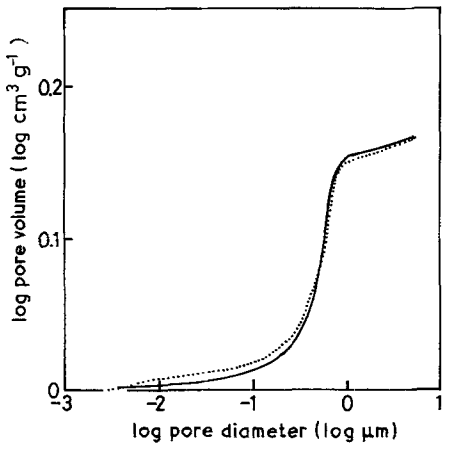

Figure 3 Pore-size distribution curves of FZP. (——) Disc burnt at 1000° C, (– – –) disc dried at 60° C.

height of the semicircle, α the depression parameter ($\theta = \pi\alpha/2$) and $j = -1^{1/2}$. The equivalent circuit corresponding to the impedance spectrum of Fig. 4 consists of a frequency dependent capacitor, $C_P(\omega)$, and a frequency independent resistor, R_P. These parameters are described by the following equations

$$Z_0 = R_P \quad (2)$$

$$C_P(\omega) = C_0(j\omega/\omega_0)^{-\alpha} \quad (3)$$

$$R_P C_0 \omega_0 = 1 \quad (4)$$

The limiting case of $\theta = 0$ represents an equivalent circuit consisting of lumped R–C components with a zero depression angle.

The value of θ for AZP estimated by complex impedance analysis is considerably larger than that of CZP and FZP and poorly dependent on the humidity, as shown in Table II. The value of θ for crystalline samples was poorly dependent on the particle size.

While the capacitive component, C_0, obtained by using Equations 3 and 4 is poorly dependent on the humidity as shown in Table III, the resistive component R_P decreases with increasing humidity for all samples. In addition, it is confirmed that the impedance at 1 kHz is approximated to the resistive component inserted parallel to the capacitive component in the humidity region above 20% r.h.

3.5. Humidity dependence of impedance

The humidity dependence of impedance at 1 kHz is shown in Figs 5 to 8 as a function of burning

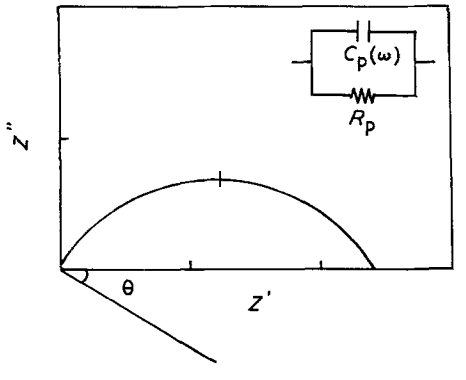

Figure 4 Complex impedance plot and equivalent circuit, notations as in text.

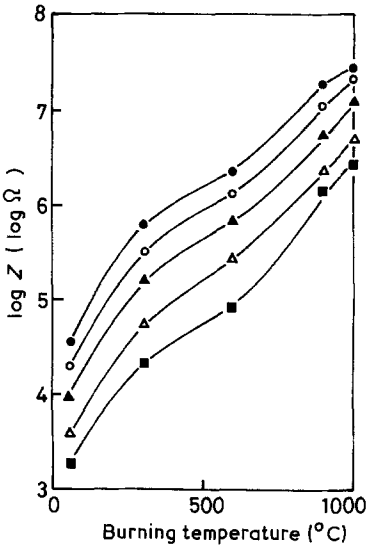

Figure 5 Burning temperature dependence of impedance of AZP. (●) 20% r.h., (○) 40% r.h., (▲) 60% r.h., (△) 80% r.h., (■) 90% r.h.

temperature. All measurements taken went from the lowest to the highest relative humidity. While the impedance of AZP increases steeply with increasing burning temperature, for CZP and FZP no similar dependencies are observed and the impedance at each humidity is lowered with decreasing particle size, i.e. an increase in surface area.

3.6. Response to humidity changes

As mentioned above, by using the method of mixing dry and moist air, stational humidity is obtained within 2 min of setting a certain humidity. Figs 9 and 10 show the impedance responses for humidity changes from 60% r.h. to 90% r.h. and vice versa. For AZP, the response time is considerably longer than that for CZP and FZP and is quickened by raising the burning temperature. Similar tendencies are confirmed over the whole humidity region for all samples. In addition, it is confirmed that the response time is prolonged by the addition of AZP to CZP.

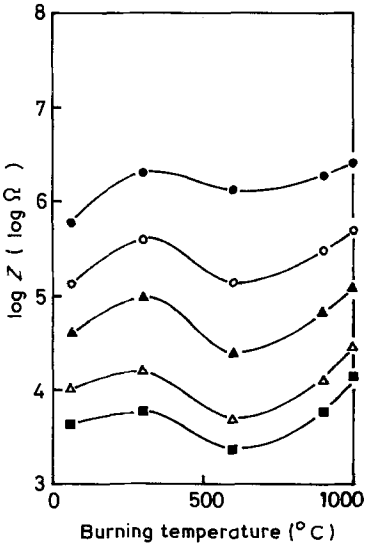

Figure 6 Burning temperature dependence of impedance of CZP100. (●) 20% r.h., (○) 40% r.h., (▲) 60% r.h., (△) 80% r.h., (■) 90% r.h.

TABLE II θ value in complex impedance plot

Sample	Burning temp. (° C)	θ (degree) at humidity of:					
		10% r.h.	20% r.h.	40% r.h.	60% r.h.	80% r.h.	90% r.h.
AZP	60	23	22	26	28	33	35
	300	31	26	28	29	29	33
	600	41	31	30	31	33	34
	900	–	15	24	24	24	25
	1000	–	–	17	24	24	22
CZP100	60	7	6	6	8	9	–
	300	12	11	11	8	8	–
	600	10	8	8	8	9	–
	900	8	8	9	9	8	6
	1000	–	7	8	9	10	8
FZP	60	–	11	9	10	9	10
	300	8	10	12	9	10	11
	600	–	7	7	7	9	8
	900	–	9	8	8	8	9
	1000	–	9	7	7	8	6

4. Discussion

4.1. Amorphous zirconium phosphate

The structure of AZP dried at 60° C may be expressed as follows [9]:

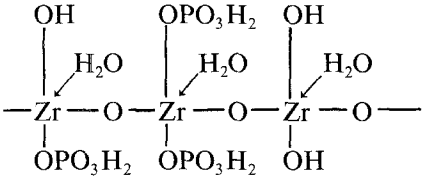

i.e. $ZrO(H_2PO_4)_x(OH)_{2-x}H_2O$. By assuming that the dehydration and the condensation of adjacent phosphate groups go essentially to completion on heating to ~800° C, the composition of the sample at each temperature is predicted from the results of the pH titration measurements and the thermogravimetric analysis. These experiments suggest that the following reactions take place,

$$ZrO(H_2PO_4)_{0.3}(OH)_{1.7}H_2O \xrightarrow[\sim 200^\circ C]{} ZrO_{1.85}(H_2PO_4)_{0.3} \xrightarrow[\sim 550^\circ C]{} ZrP_{0.3}O_{2.75}$$

It is clear that these compositional changes are accompanied by the disappearance of an amorphous phase and the appearance of the crystalline phase, as shown in Figs 1 to 3. As mentioned above, the response time is prolonged by the addition of amorphous zirconium phosphate to crystals of zirconium phosphate. Therefore, it is concluded that for the preparation of a humidity sensor with a fast response time, it is necessary to prepare fine-grained crystalline zirconium phosphate. As shown in Fig. 5, the impedance at each humidity increases steeply with increasing burning temperature.

It is well known that the admittance of porous ceramics without any mobile carriers is usually enhanced by adsorption of water and/or capillary condensation of water [10, 11]. When water molecules are present on the surfaces of porous ceramics, but surface coverage is not complete, H_3O^+ diffusion and H^+ hopping and/or transfer occur. When water molecules are abundant, the physisorbed water dissociates because of the high electrostatic field in the chemisorbed water: $2H_2O \rightleftharpoons H_3O^+ + OH^-$. Charge transport occurs when an hydronium ion releases a proton to the neighbouring water molecule (Grotthuss chain reaction). In

TABLE III C_0 values

Sample	Burning temp. (° C)	C_0(pF cm^{-1}) at humidity of:					
		10% r.h.	20% r.h.	40% r.h.	60% r.h.	80% r.h.	90% r.h.
AZP	60	–	6	7	10	–	–
	300	–	12	13	15	16	17
	600	–	12	12	13	14	15
	900	–	–	–	5	5	5
	1000	–	–	–	–	6	5
CZP100	60	–	2.0	2.0	2.1	–	–
	300	2.5	2.4	2.1	2.0	–	–
	600	1.8	2.0	1.9	1.8	–	–
	900	1.8	2.1	2.3	2.2	–	–
	1000	–	1.9	1.9	1.7	–	–
FZP	60	–	2.0	2.5	2.3	2.5	2.4
	300	2.6	2.3	2.3	2.0	2.3	2.2
	600	–	1.6	1.7	1.6	1.7	1.8
	900	–	2.0	1.8	1.8	1.7	2.0
	1000	–	2.2	1.8	1.7	1.6	1.6

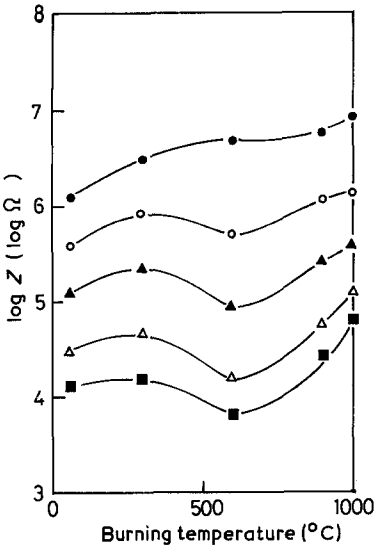

Figure 7 Burning temperature dependence of impedance of CZP400. (●) 20% r.h., (○) 40% r.h., (▲) 60% r.h., (△) 80% r.h., (■) 90% r.h.

these cases, it is expected that the admittance in a humid atmosphere will be proportional to the surface area and the amount of adsorbed water when the coverage of physisorbed water is larger than 2 [11, 12]. However, for amorphous zirconium, such a relationship is not confirmed. This discrepancy may be caused by the existence of strongly acidic protons. In this case, the carrier may be produced not only by the dissociation of physisorbed water but also by the dissociation of the strongly acidic protons (PO–H). If the strongly acidic proton for the phosphorus atom exists in a perfectly dissociated form and its concentration is much larger than that of the carrier produced by the dissociation of physisorbed water, the carrier concentration is approximated to that of the strongly acidic proton for the phosphorus atom:

$$n = [\text{PO–H}] \quad (5)$$

If the proton transport is governed by the jump probability of proton into the trapping and/or hopping sites, the jump frequency, ω_J, depends upon the

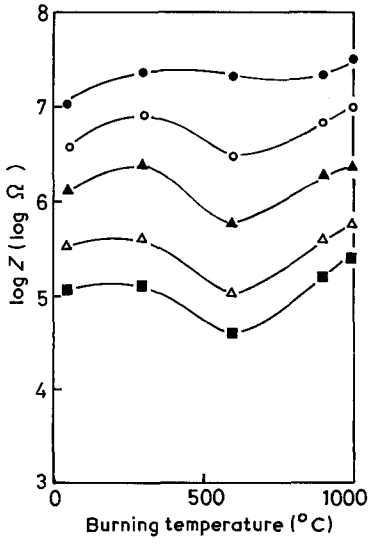

Figure 8 Burning temperature dependence of impedance of FZP. (●) 20% r.h., (○) 40% r.h., (▲) 60% r.h., (△) 80% r.h., (■) 90% r.h.

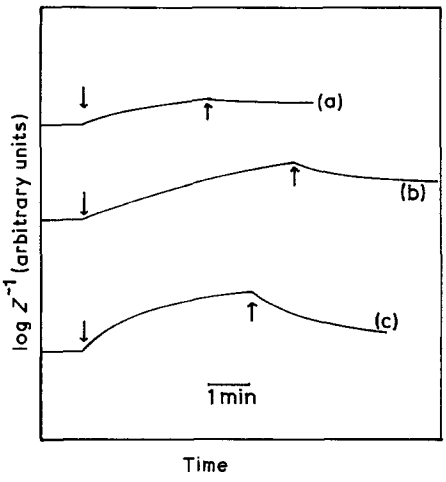

Figure 9 Impedance response for humidity changes from 60% r.h. to 90% r.h. and vice versa. (↓) 60% r.h. → 90% r.h., (↑) 90% r.h. → 60% r.h. (a) AZP dried at 60° C, (b) AZP burnt at 600° C, (c) AZP burnt at 1000° C.

potential barrier expressed as

$$\omega_J = \nu_0 \exp(\Delta S/k) \exp(-\Delta H/kT) \quad (6)$$

where ν_0 is the vibrational frequency for a carrier, ΔS is the entropy of migration and ΔH is the enthalpy of migration. For this system, the adsorbed water should act as a trapping and/or hopping site for the mobile protons. Finally, the conductivity, σ, is given by

$$\sigma = na^2e^2\omega_J/kT \quad (7)$$

where a is the jump distance and e is the charge element. In a previous paper [13, 14], it was reported that the impedance at each humidity is inversely proportional to the surface concentration of strongly acidic proton for the burnt zircon with phosphoric acid. In Fig. 11, the relationship between impedance and concentration of strongly acidic proton is shown. For the sample burnt at 600° C or below, the impedance is inversely proportional to the concentration of strongly acidic proton, but for the sample burnt at 900° C, a deviation from this expected relationship is observed. Because the surface area of the sample burnt at 900° C is very much smaller than that of the samples

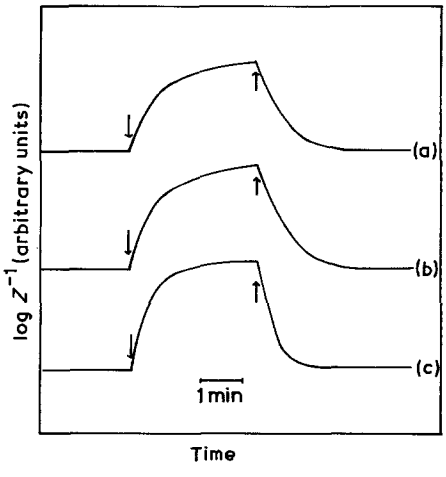

Figure 10 Impedance response for humidity changes from 60% r.h. to 90% r.h. and vice versa. (↓) 60% r.h. → 90% r.h., (↑) 90% r.h. → 60%r.h. (a) FZP dried at 60° C, (b) FZP burnt at 600° C, (c) FZP burnt at 1000° C.

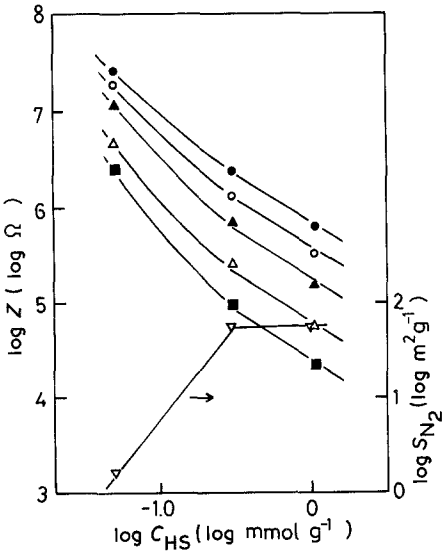

Figure 11 C_{HS} dependence of impedance and relationship between surface area and C_{HS} for AZP. (●) 20% r.h., (○) 40% r.h., (▲) 60% r.h., (△) 80% r.h., (■) 90% r.h.

burnt at 600° C or below, this deviation can be qualitatively realized by the difference of surface area as shown in Table I and Fig. 11.

4.2. Crystalline zirconium phosphate with a layered structure

Assuming that the weight loss by heat treatment is caused by the dehydration and condensation of adjacent phosphate groups and that these reactions go essentially to completion on heating to ~800° C, the compositional structure of the sample is assigned as follows with the aid of X-ray diffraction analysis and thermal gravimetric analysis,

$$\alpha\text{-}Zr(HPO_4)_2H_2O \xrightarrow[\sim 450^\circ C]{} Zr(HPO_4)_2$$

$$\xrightarrow[\sim 600^\circ C]{} ZrP_2O_7$$

In addition, it is confirmed that the concentration

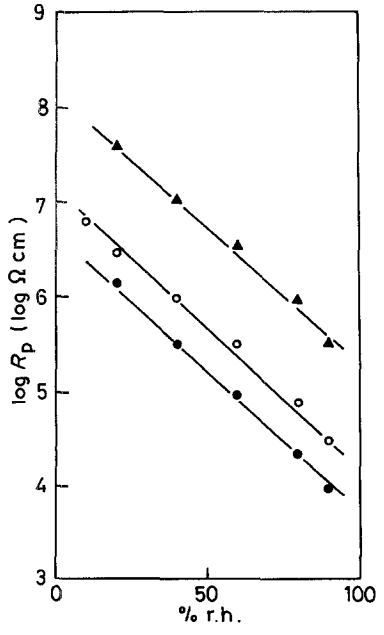

Figure 12 Humidity dependence of R_P for disc dried at 60° C. (●) CZP100, (○) CZP400, (▲) FZP.

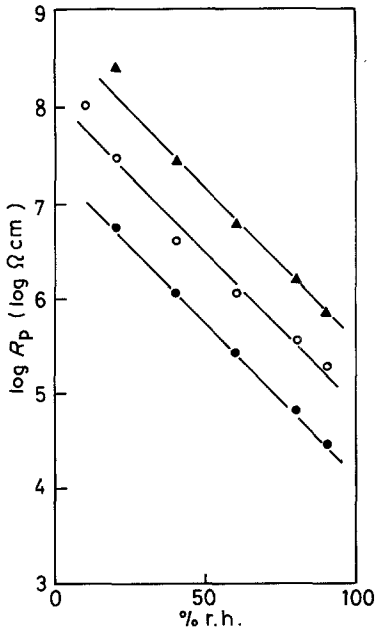

Figure 13 Humidity dependence of R_P for disc burnt at 1000° C. (●) CZP100, (○) CZP400, (▲) FZP.

of the strongly and weakly acidic protons decreases on heating to ~600° C, while the geometrical structure (particle size and form) is scarcely dependent on the burning temperature. In Fig. 3, the pore-size distribution curves for the compressed powder discs of crystalline zirconium phosphate are shown. No distinct difference in the pore-size distribution curve can be detected. These observed results convinced us that the results of surface area, determined by the BET method using nitrogen as a sorbate, were correct.

The relationship between resistivity, determined by complex impedance analysis, and humidity is shown in Figs 12 and 13. The absolute value of resistivity decreases with decreasing average particle size, while the slope in this relationship is poorly dependent on the particle size.

The relationship between resistance at 90% r.h. and concentration of strongly acidic proton is shown in Fig. 14. A distinct proton concentration dependence of resistivity and/or impedance as observed in the AZP system is not confirmed.

For zirconium *bis*(monohydrogen orthophosphate)-

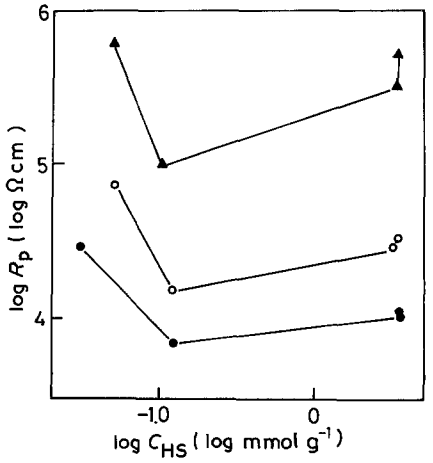

Figure 14 Relationship between R_P at 90% r.h. and C_{HS}. (●) CZP100, (○) CZP400, (▲) FZP.

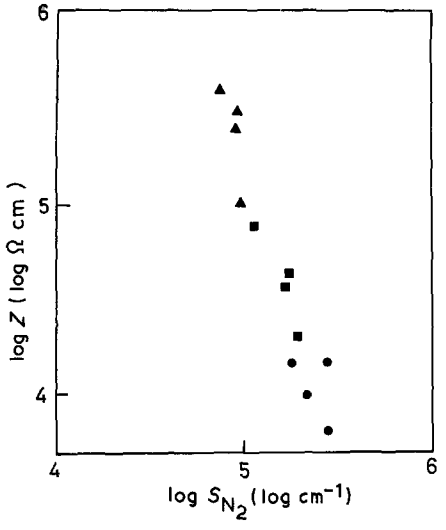

Figure 15 Relationship between impedance at 90% r.h. and surface area. (●) CZP100, (■) CZP400, (▲) FZP.

monohydrate with a layered structure, most of the acidic protons exist in the interlayer spaces, and the equivalent fraction of surface protons in the microcrystals is very small (10^{-3} to 10^{-4}) [15]. Alberti *et al.* [15] reported that the electrical mobility of surface protons was much greater than the internal ones by a factor of 10^4 or more. This means that the contribution of surface protons to the total conduction is very high. In addition, it has been reported by Casciola and Constantino [16] that the d.c. conductivity lies in the range 3 to 0.9 $\times$ $10^{-4}\Omega^{-1}cm^{-1}$ when the sheets are oriented parallel to the electrical field and are about seven times lower in the case of perpendicular orientation at 20° C and 90% r.h. In these electrical measurements, the electric field was applied perpendicular to the surfaces observed by scanning electron microscopy. As shown in Figs 1 and 2, the faces of crystalline samples with a layered structure are oriented perpendicular to the electric field and the degree of orientation increases with increasing particle size. Therefore, it is expected that the contribution of internal protons to the total conduction is very much lower than that of the surface protons (PO–H) and/or the protons produced by the dissociation of physisorbed water for this system. This expectation convinced us of the relationship between resistivity and concentration of a strongly acidic proton for a crystalline sample (Fig. 14). Previously, it has been reported [11, 12] that the admittance in a humid atmosphere is proportional to the surface area when the coverage of physisorbed water is the same for the porous ceramics prepared using fine-grained insulating materials. This relationship indicates that the effective cell constant(electrode area/interelectrode distance) is linearly proportional to the surface area of porous ceramics in which most of the pores consist of through pores. However, for the crystals with a layered structure which oriented perpendicular to the electric field, it seems that the effective cell constant is considerably smaller than that expected from the surface area. Fig. 15 shows the relationship between resistance and surface area determined by the BET method. The slope of the solid line in the relationship between log resistance and log surface area, is considerably higher than that of the relationship confirmed in the porous ceramics reported in previous papers [11, 12]. This indicates that the effective cell constant for conduction is lowered with increasing particle size, because the faces of the layers in the crystal are oriented perpendicular to the electric field. From these confirmed results, it is concluded that the fine-grained crystalline zirconium phosphate is the preferable material for use as a humidity sensing device in respect of the humidity sensitivity and the response to humidity changes.

Acknowledgements

We thank K. Ishizawa and his co-workers of Shinagawa Refractories Co. for technical assistance.

References

1. M. HIJIKIGAWA, S. MIYOSHI, T. SUGIHARA and A. JINDA, *Sensors and Actuators* **4** (1983) 307.
2. Y. SAKAI and Y. SADAOKA and K. IKEUCHI, *ibid.* **9** (1986) 124.
3. C. B. AMPHLETT, L. A. McDONALD and M. J. REDMAN, *J. Inorg. Nucl. Chem.* **6** (1958) 220.
4. A. DYER, D. LEIGH and F. T. OCON, *ibid.* **33** (1971) 3141.
5. S. YDE-ANDERSEN, J. S. LUNDSGAARD, J. MALLING and J. JENSEN, *Solid State Ionics* **13** (1984) 81.
6. E. KROGH ANDERSEN, I. G. KROGH ANDERSEN, C. KNAKKERGÅRD MØLLER, K. E. SIMONSEN and E. SKOU, *ibid.* **7** (1982) 301.
7. M. CASCIOLA and D. BIANCHI, *ibid.* **17** (1985) 218.
8. A. CLEARFIELD, W. L. DUAX, A. S. MEDINA, G. D. SMITH and J. R. THOMAS, *J. Phys. Chem.* **73** (1969) 3424.
9. M. ABE, *Denki Kagaku*, **48** (1980) 344.
10. T. SEIYAMA, N. YAMAZOE and H. ARAI, *Sensors and Actuators* **4** (1983) 85.
11. Y. SADAOKA and Y. SAKAI, *Denki Kagaku* **51** (1983) 879.
12. *Idem, Hyomen Kagaku* **5** (1984) 220.
13. *Idem, Denki Kagaku* **53** (1985) 896.
14. *Idem, J. Mater. Sci.* **21** (1986) 3717.
15. G. ALBERTI, M. CASCIOLA, U. CONSTANTINO, G. LEVI and G. RICCIARDI, *J. Inorg. Nucl. Chem.* **40** (1978) 533.
16. M. CASCIOLA and U. CONSTANTINO, *Solid State Ionics* **20** (1986) 69.

Received 6 October 1986
and accepted 19 January 1987